

END DETAILING EXPERIMENTAL STUDY ON THE SEISMIC PERFORMANCE OF ALL-STEEL TUBULAR BRBS

Seayf Allah Hemati^{1*}, Mohammad Ali Barkhordari Bafghi², Ali kheyroddin³

**Corresponding Author:*

Highlights:-

A new type of all-steel BRB with a steel tube as a core member is proposed.

Effects of end detailing on AST-BRBs seismic performance are investigated.

The seismic performance of an AST-BRB welded to support through its lid is satisfactory.

An AST-BRB is lighter, less costly, and easier to fabricate and erect.

AST-BRBs can be used as a suitable alternative to conventional bracing in engineering applications.

Abstract:-

To clarify the effects of end details on the seismic performance of a new type of All-Steel Tubular Buckling Restrained Brace (AST-BRBs) constructed by placing a steel tube as a core member within another steel tube as an external restraint (pod), an experimental study was conducted. Seismic behaviors of six specimens (two non-pod and four pod specimens) with three different end detail specifications were studied under cyclic loads. The experimental results show that AST-BRBs with end portions sent through a tube gradually increase in diameter with a lid welded to the end support plate. In addition to satisfying specified requirements, compared with the non-pod specimen, the specimen with a pod can dissipate over 13 times more energy and offers a compressive bearing capacity of more than 2.2 times that of a nominal load capacity. Therefore, the seismic performance of this type of BRB is satisfactory and, due to their low cost, can be used as a suitable alternative to conventional bracing in engineering applications and steel structures.

Keywords:- *Buckling restrained brace, Compressive bearing strength, Seismic performance, Hysteretic behavior, and All-steel tubular brace.*

1. INTRODUCTION

Past research studies have shown that Buckling Restrained Braces (BRBs) efficiently improve building performance in seismic areas owing to their high energy dissipation capacities and ductility. For this reason, various types of BRBs have been examined by several researchers. In turn, (i) over the past thirty years the behaviors of such braces have been closely investigated both experimentally and numerically based on the hysterical behaviors of concrete-steel composition elements that can be useful in terms of energy dissipation [1-15]; (ii) many existing structures that are highly vulnerable to seismic events have been retrofitted with BRB systems [16-22]; and (iii) regulations and conditions common of their use are noted in modern seismic codes [23-25].

Most conventional BRBs are composed of an encasing core steel member confined by infill concrete and placed into a steel hollow structural section. Other BRBs include all-steel BRBs, which consist of a steel plate as a core member and external restraining steel elements connected by welds or bolts. Compared to conventional BRBs, all-steel BRBs present numerous advantages, (i) presenting few problems during installation and (ii) being inexpensive to use due to being light in weight and due to not requiring the use of special technologies for their construction and installation [26-36].

A novel All Steel Tubular Buckling Restrained Brace (AST-BRB) composed of two circular steel tubes of different diameters is proposed. AST-BRBs are constructed by placing a steel tube as a core member within another steel tube as an external restraining member (pod) to prevent the pod from causing out-of-plane buckling in the core member. Such braces can be considered ordinary all-steel BRBs with enhanced characteristics in terms of removing bolts and welds during fabrication and in terms of preventing local buckling along tubes. They are also easy to fabricate and erect, remove frictional forces at the contact interface between core members and pods and thus simplify the design process, rendering them more economical.

Three improvements to end details of AST-BRBs are proposed. For the first and second improvements specimen end details are designed to evaluate the effects of core member end rotation on the seismic performance of AST-BRBs and on ease of implementation.

We examined six specimens divided into quadruple and dual specimens and tested under axial cyclic loading. Effects of end region detailing on specimen seismic performance were investigated in terms of index deformation and failure modes, hysteretic behaviors, energy dissipation levels and compressive bearing strength values. Finally, the most suitable end specifications for the fabrication of AST-BRBs are proposed.

In the following sections stages of the present research project are described and results obtained from the test specimen are compared. Finally, an appropriate option is identified.

2. Experimental program

2.1 Material testing, design and fabrication of specimens

Tubes with diameters of 3/4 and 1, 1/4 inches are considered as specimen cores. Coupon tests are carried out to determine tensile stress-strain characteristics of the selected tube. Based on the results of these tests, we have, $f_y=360\text{MPa}$, $f_u=450\text{MPa}$ for tube of 3/4 and $f_y=240\text{MPa}$, $f_u=360\text{MPa}$ for tube of 1, 1/4, such that f_y and f_u are the yield stress and ultimate stress, respectively.

In accordance with materials properties and provisions for structural steel buildings established by the American Institute of Steel Construction (AISC 360-16) [25], to limit overall buckling in the core member, laterally unbraced lengths of the core member, L , are determined as follows:

$$L = \frac{4.71r}{k} \sqrt{\frac{E}{f_y}} \quad (1)$$

Where r is the radius of the gyration of the member, where is the effective length factor for flexural buckling, and where E is the modulus of elasticity of steel used?

Lengths of the core members of specimens are designed such that the slenderness coefficient of the core member is equal across all specimens. The pod is shorter than the core member to prevent the transmission of axial deformation to the pod, which can transmit the axial force of the core member to the pod during testing.

The diameter of the pod is determined to minimize the distance between pods and the core while the core member moves easily within the pod. Core members of the first and second parts of the specimens are a tube of 3/4" with $f_y=360\text{MPa}$ and tube of 1, 1/4" with $f_y=240\text{MPa}$, respectively.

The first specimens include a NP1-SBRB (Fig. 1a), which is non-pod prototype specimen, and three specimens of NWS-BRB (Fig. 1b), PES-SBRB (Fig. 1c) and CP1-LBRB (Fig. 1d), which are covered with a pod and which are AST-BRB specimens. The second specimens include NP2-LBRB (Fig. 1e), a non-pod prototype specimen, and CP2-LBRB (Fig. 1f), which is covered with pods as an AST-BRB specimen.



Fig. 1 Photos of the test specimens

End details of the first specimens are constructed based on proposed specifications and those of the specimens re similar to the first specimens given their suitable performance as shown by our test results. The end region of NP1-SBRB includes three support stiffening segments to connect each end of the core member to the end plate (Fig. 2a). Both end regions of core members of the NWS-BRB and PES-SBRB specimens are reinforced by welding four longitudinal stiffening plates to keep the specimens elastic. At the two extreme edges of the pod of the PES-SBRB specimen, four slots are included to allow longitudinal stiffening plates to move freely into the slots during testing and the compressive axial force is not transferred from the core member to the pod. Through full penetration welding both ends of the core tubular member of the NWS-BRB specimen are connected to the end plate (Fig. 2b), but for the PES-SBRB specimen in addition to full penetration welding three support stiffening segments are used for connections (Fig. 2c). In the NP2-LBRB, CP1-LBRB and CP2-LBRB specimens both end regions of core members of the longitudinal stiffening plates and support stiffening segment are replaced with a steel lid with a cross-sectional variable and with a diameter gradually extending from ends of the core member to the end plate (Fig. 2d-2f). Specifications of the specimens are presented in Fig 2, in which geometric and design dimensions of the test specimens are presented.

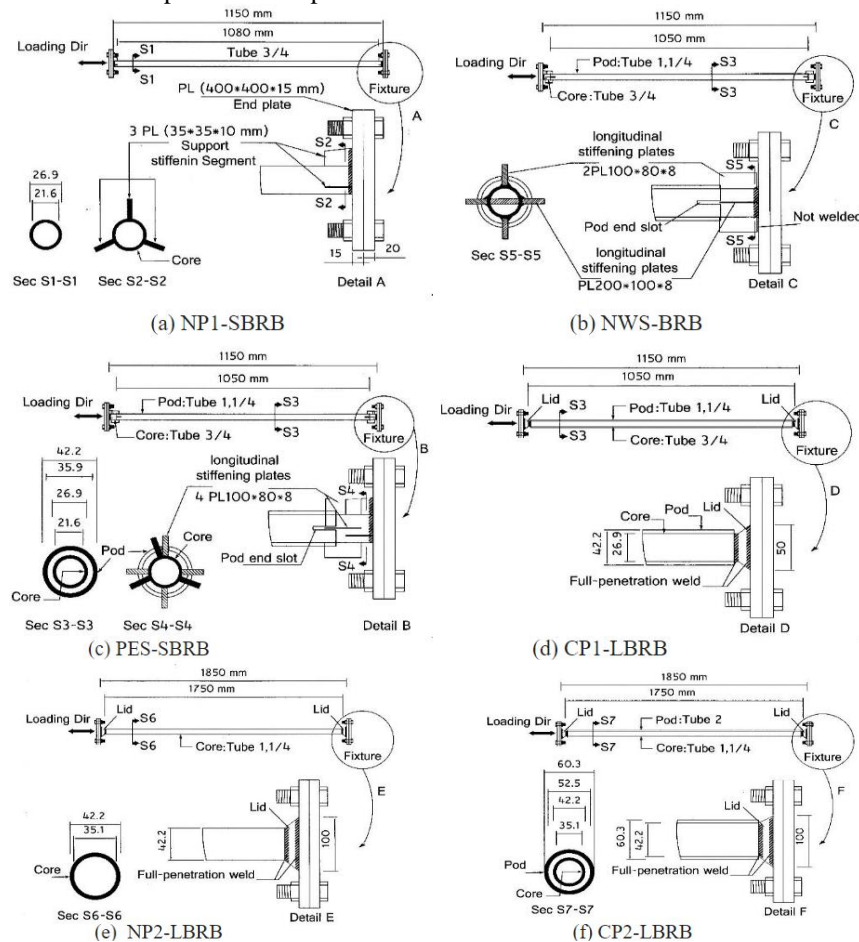


Fig.2 Schematic of the specimens

2.2 Test setup and axial cyclic loading

To better understand the seismic behavior and compressive bearing strength of AST-BRBs, axial cycle loading tests were conducted on the specimens. The test setup includes the specimen, strong bases, a tension and compressive actuator, measuring instruments, and a data logger device assembled through a suitable and reliable method prior to testing

(prepared at the Structural Laboratory of Semnan University, Iran). One end of the specimen is connected to the loading device by the end plate and fixture while the other end of the specimen is connected to strong bases by the end plate. The actuator is applied in the specimen's axial direction. The axial load is measured by a load cell while the axial displacement of the specimens is measured by displacement transducers (LVDTs) placed on both plates as shown in Fig. 3.

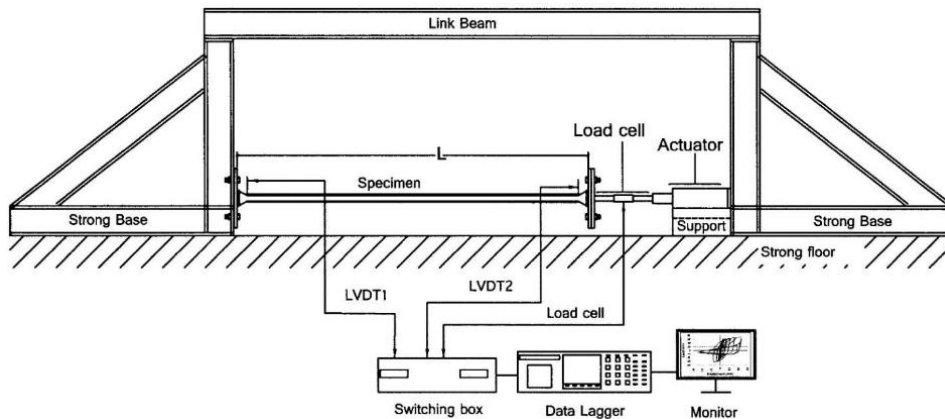


Fig.3. Setup used for testing

Axial cyclic loadings of the specimens based on different end details and depending on core members are covered with pods or include no pods and vary slightly. Cyclic axial load values measured by the load cell to each of specimens are illustrated in Fig. 4. The vertical coordinate is the applied axial load of the specimen with the sign convention of tension being positive and with that of compression being negative. The horizontal coordinate denotes the loading cycle value.

3. Test results

3.1 Damage and rupture modes of the AST-BRB

Fig. 5 presents damage modes of the specimens. The PES-SBRB specimen is found to undergo local damages due to weaknesses observed at the ends of pods resulting from the presence of slots (fig. 5a, 5b). At the end of the core member of the NWS-BRB specimen we also find higher levels of external core bending and potentially due to the removal of the support stiffening segment and non-connecting longitudinal stiffening plate edge from the end plates (Fig .5c) whereas the other test specimens undergo overall buckling damage (Fig .6). Specimens rupturing is show to spur tensile stress while specimens are subjected maximum bearing capacity and as applied loads decrease.

The CP1-LBRB and CP2-LBRB specimens with lid end details present more reasonable signs of deformation than the other specimens, and lid is effective at subjecting the weak regions of specimens overall buckling damage rather to local damage. Up to the failure point (i.e., core rupture), no rupturing in lid welds occurs. No core instability nor core member-to-end plate connection rupturing is observed in these types of AST-BRBs. Fig.7 shows the positions of core ruptures observed in the specimens.

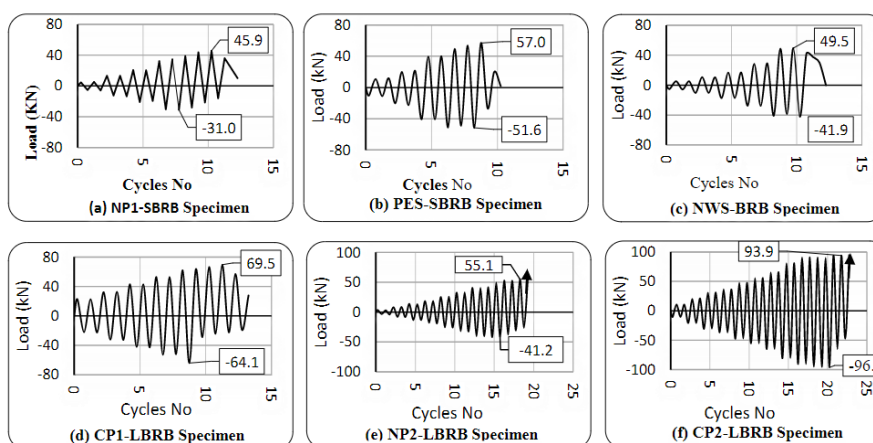


Fig. 4. Specimen cyclic loading schemes

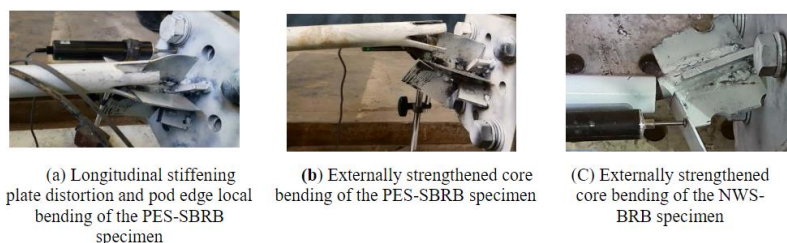


Fig.5. Local damage to the specimens at the end of compression loading



Fig.6. Overall buckling figures of specimens at the end of the test.

3.2 Stress-strain and backbone curves of the specimens

A thorough analysis of the stress-strain curves of the specimens derived from seismic performance indices of the proposed BRBs (AST-BRBs) can be obtained (e.g., the compressive strength adjustment factor, the cumulative energy dissipation index and the bearing capacity of specimens). Stress-strain and backbone values of the specimens are shown in Fig. 8. The vertical coordinate is the applied stress of the specimen with the sign convention of tension being positive and with that of compression being negative. The horizontal coordinate is the measured strain value with the same sign convention. As is shown in Fig. 8, for the specimens covered with pods and especially for CP1-LBRB and CP2-LBRB specimens compared to non-pod specimens, plump hysteresis curves show stable hysteretic and repeatable behavior with no signs of strength and stiffness degradation. For these specimens stiffness values in the post yield region increase slightly and mainly due to the strain hardening effect.



Fig.7. Core rupture positions observed in the specimens

I. Compressive strength adjustment factor

Asymmetries of the hysteresis curves may cause the cross-section of a core member to expand under compression due to the Poisson effect. Conversely, they tended to decrease under tension, thus leading to asymmetrical behavior based on the loading direction. Additionally, end detailing can support asymmetric hysteretic performance in specimens. Asymmetries in tension and compression responses of a BRB are usually evaluated from the compressive strength adjustment factor, β which is obtained from a qualification test data backbone curve. It is defined as:

$$\beta = \frac{\sigma_{cmax}}{\sigma_{tmax}} \quad (2)$$

where σ_{tmax} is the maximum tension stress value corresponding to $1.5\Delta_{by}$, where σ_{cmax} is the maximum compressive stress value of the core member, and Δ_{by} is the total axial deformation value based on the first significant yield of the test specimen. The value of β shall not exceed 1.3 and in no case shall be taken as less than 1.0 based on ANSI/AISC 341-10 (AISC, 2010) [24]. The range of a typical value of β is 1.05 to 1.15 [25]. Compressive adjustment factors of the test specimens are compared in Table 1.

The data presented in Table 4 show that the PES-SBRB, CP1-LBRB and CP2-LBRB specimens exhibit symmetrical and stable hysteretic behavior throughout the loading process. In addition, the coefficient β for these specimens remains at less than 1.3 and therefore these specimens satisfy seismic provisions of the AISC code.

Table 1. Comparison of the compressive adjustment factor parameters, β

Specimen	NP1-SBRB	NWS-BRB	PES-SBRB	CP1-LBRB	NP2-LBRB	CP2-LBRB
σ_{tmax} (Mpa)	210.4	209.2	227.2	259.5	134.6	197.3
σ_{cmax} (Mpa)	141.9	184.1	236.7	294.2	94.4	223.6
β	0.67	0.88	1.04	1.13	0.7	1.13

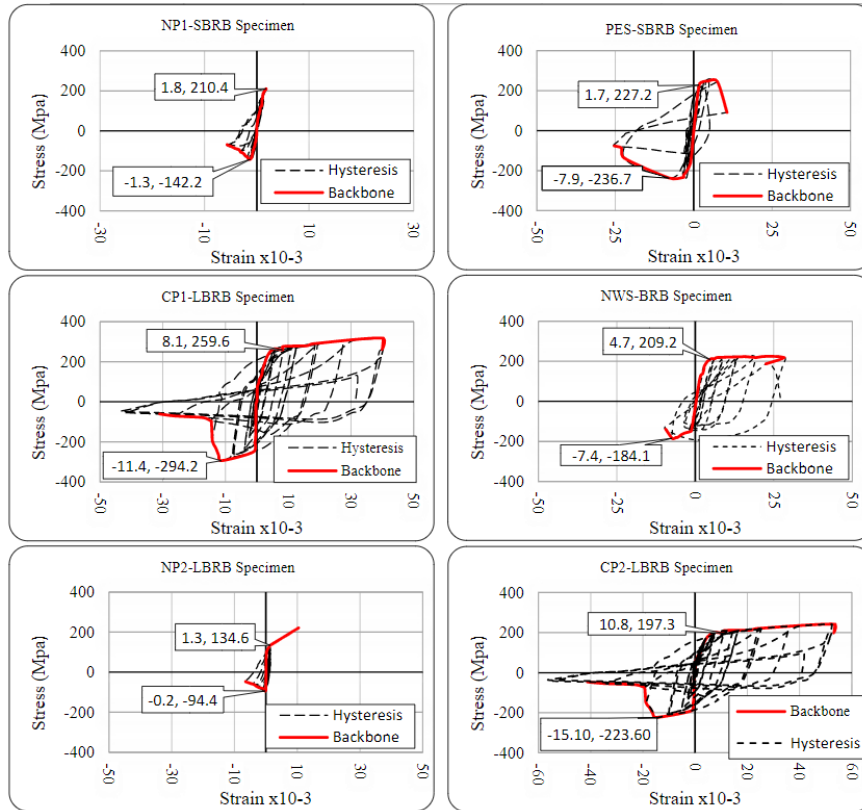


Fig.8. Stress- strain and backbone curves

II. Evaluation of cumulative dissipated elastic energy levels

Cumulative dissipated energy levels can reflect a specimen’s capacity to absorb seismic energy, which can be used to evaluate the seismic behavior of test specimens. The cumulative dissipated elastic energy level of each test specimen can be calculated by measuring the total area under the load–displacement curve bounded by the elastic zone (Fig. 9(a)–(f)). The total cumulative dissipated elastic energy value for each specimen (TDE) is calculated in Table 2

To determine the best end details of the proposed specimen, based on dissipated energy levels, the dissipated energy ratio for test specimen with core member of 3/4" (DERs) can be calculated from Eq. (4) And for test specimen with core member of 1, 1/4" can be calculated from Eq. (5) as follows:

$$DER_s = \frac{TDE_s}{TDE_{NP1}} \tag{4}$$

$$DER_L = \frac{TDE_L}{TDE_{NP2}} \tag{5}$$

Where TDE_s and TDE_L denote the total cumulative dissipated elastic energy level derived from small and large specimens, respectively. TDE_{NP1} , and TDE_{NP2} denote total cumulative dissipated elastic energy levels for the NP1-SBRB and NP2-SBRB specimens, respectively. Comparative results are presented in Table 2.

As indicated in Table 2, the energy dissipation capacity of specimens PES-SBRB and NWS-BRB (as an initial proposal for AST-BRB) and specimens NP1-LBRB and NP2-LBRB (as a control specimens) is much less than that of specimens CP1-LBRB and CP2-LBRB (which the steel lid are welded at their both ends and have pods). In other words, specimens CP1-LBRB and CP2-LBRB will be able to absorb the largest amount of energy. Hence, it can be concluded that these specimens can be used as AST-BRB and energy absorption systems in engineering applications.

Table 2. Comparison of dissipated energy ratios of the test specimens

Specimen	NP1-SBRB	PES-SBRB	NWS-BRB	CP1-LBRB	NP2-LBRB	CP2-LBRB
TDE (Mpa.mm/mm)	179	859	735	2817	533	7015
DER	DER _s			DER _L		
	1.0	4.8	4.1	15.7	1.0	13.2

III. Determination of increases in compressive bearing strength

To clarify the influence of pod installation and end details on the compressive bearing strength of AST-BRBs, a normalized expression of the compressive bearing strength index is used as defined by Eq.(6):

$$\eta = \frac{P_{max}^c - P_n^c}{P_n^c} * 100 \quad (6)$$

Where P_{max} is the maximum compressive strength value obtained from the test specimen (Fig.4) and where P_n^c is the nominal compressive strength of specimens, which is determined in accordance with applicable limit states of the flexural buckling of provisions for structural steel buildings defined by the American Institute of Steel Construction (AISC 360-16) [23]. The coupon test results given in section 3.1 show that nominal compressive axial strength values of the individual core cross-section for tubes 3/4 and 1,1/4 are computed as 29.8kN and 40.9 kN, respectively. Values η are presented in Table 3.

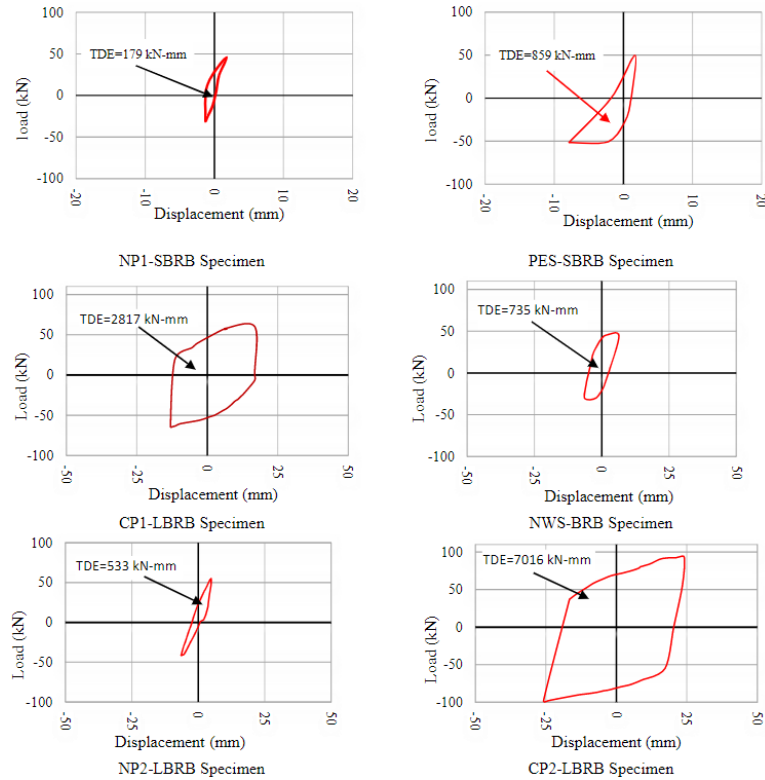


Fig. 9. Cumulative dissipated energy within the elastic range of the test specimens.

Table 3. Compressive bearing strength indexes (of the test specimens)

Specimen	NP1-SBRB	PES-SBRB	NWS-BRB	CP1-LBRB	NP2-LBRB	CP2-LBRB
P_n^c	29.8	29.8	29.8	29.8	40.9	40.9
P_{max}^c	31	52.6	41.9	64.1	41.2	96
η %	4.0	76.5	40.6	115.1	0.7	134.7

It can be deduced from Table 3 that when a pod is placed around a core member and even in a NWS-BRB specimen with a weak end connection, an at least 40% increase in compressive bearing strength is observed. The creation of suitable end conditions for the CP1-BRB and CP2-BRB specimens through the installation of a core member lid as a transfer region led to increases compressive bearing strength of up to 115% and 134%, respectively (more than twice the nominal compressive strength of the specimens).

4. Conclusion

In an experimental study, cyclic loading tests of six AST-BRB specimens as new types of all-steel BRBs with different yield strength values are performed to examine the influence of pod installation and three forms of end detailing on hysteretic behaviors, damage and rupture modes, and energy dissipation capacity.

From this study the following conclusions can be drawn:

- [1]. Depending on different pod erection approaches and end connection specifications used, AST-BRBs can dissipate approximately 4–13 times more energy than non-pod specimens.
- [2]. The overall and local buckling conditions of the AST-BRB are dependent on such factors as the following: (i) geometric characteristics and mechanical properties of pods, (ii) distances between core members and pods and (iii) end details such as pod slot ends, geometric characteristics of longitudinal stiffening plates on the core member, and connection features.

- [3]. When there are slots at the end of a pod, the core member end of the PES-SBRB specimen will easily undergo pod end local bending damage. This damage mode can be avoided by applying reasonable construction measures.
- [4]. AST-BEBs with lid end connections serving as transitional regions (CP1-LBRB and CP2-LBRB specimens) generate better results than the other two proposed end details (PES-SBRB and NWS-BRB specimens) in terms of damage and rupture modes, hysteretic behaviors, stable and repeatable hysteretic curves, energy dissipation performance and compressive bearing strength. Accordingly, in engineering applications these can be used for all-steel BRBs.

REFERENCES

- [1]. Y-L. Guo, J-Z. Tong, X-A. Wang, B-H. Zhang, Subassemblage tests and numerical analyses of buckling-restrained braces under pre-compression, *Engineering Structures*, Volume 138, (1 May 2017), Pages 473-489.
- [2]. H.Sugihardjo, Tavio, Cumulative ductility and hysteretic behavior of small buckling-restrained braces, *Advances in Civil Engineering*, Volume2017, (2017), Article ID7105768.
- [3]. M. Gholhaki, A. Jamalifar, Investigating the Effects of the Spacing of the Steel core from Concrete Incorporated in the pod of buckling restrained braces, *Journal of Structural Engineering and Construction*, (Feb 2016).
- [4]. N. Bharath Gowda, R. K. Chethan Gowda, N. Nayana Patil, Experimental and analytical studies of 3D, *International Journal of Civil Engineering and Technology*, Volume7, Issue 5, (September-October 2016), pp. 78–86, Article ID: IJCIET-07-05-010.
- [5]. J.Shen, O. Seker, N. Sutchiewcharn, B. Akbas, Cyclic behavior of buckling-controlled braces, Volume 121, (June 2016) , Pages 110-125.
- [6]. Z. Jiang, Y.Guo, B.Zhang, X.Zhang, Influence of design parameters of buckling-restrained brace on its performance, *Journal of Constructional Steel Research*, Volume 105, (, February 2015) Pages 139-150.
- [7]. A. Kheyroddin, A. Mortezai, R. Aghili, Investigating the behavior of metal buckling restrained braces in improving the seismicity of RC structures, *Journal of Civil Engineering*, Vol. 15, No. 1(2015).
- [8]. S.A. Razavi, S.R. Mirghaderi, A. Hosseini, Experimental, and numerical developing of reduced length buckling-restrained braces. *Engineering Structures*, Volume 77(15 October 2014), Pages 143–160.
- [9]. A. Rahai, M. Mortazavi, Experimental and numerical study on the effect of core shape and concrete cover length on the behavior of BRBs, *International Journal of Civil Engineering*, Vol. 12, No. 4, (December 2014) *Transaction A: Civil Engineering*.
- [10]. F. Arbabi, M. Tabarok, An experimental study on one of the all Steel Buckling Restrained Brace (S-BRB), *Journal of Science & Research*. Vol. 46, No. 2, (Winter 2014), Pages 53-55.
- [11]. T. Takeuchi, J.F. Hajjar, R. Matsui, K. Nishimoto, I.D. Aiken, Effect of local buckling core plate restraint in buckling restrained braces, *Engineering Structures* Volume 44 (2012) 304–311.
- [12]. F. López-Almansa, J.C. Castro-Medina, S. Oller, A numerical model of the structural behavior of buckling-restrained braces, *Engineering Structures*, Volume 41, (August 2012), Pages 108-117.
- [13]. G.S. Prinz, P. W. Richards, Seismic performance of buckling-restrained braced frames with eccentric configurations, *Journal of structural engineering*, (March 2012), Pages 345-353.
- [14]. C-Che. Chou, S-Y. Chen, Subassemblage tests and finite element analyses of sandwiched buckling-restrained braces, *Engineering Structures*, Volume 32, Issue 8, (August 2010), Pages 2108-2121.
- [15]. A. Kheyroddin, S. Moheb shahedin, Comparison of the results of the analysis of the overload analysis of structures by unrestrained and conventional braces, In: 7th International Congress on Civil Engineering, Tarbiat Modares University, Tehran, 2006.
- [16]. P-C. Lin, K-C. Tsai, A-C. Wu, M-C. Chuang, C-H. Li, K-J. Wang, Seismic design and experiment of single and coupled corner gusset connections in a full-scale two-story buckling-restrained braced frame, *Earthquake Engineering and Structural Dynamics*, Volume 44 issue 13 , (25 October 2015) Pages 2177-2198.
- [17]. J.Zhao, F.Lin, Z, Wang, Seismic design of buckling-restrained brace welded end connection considering frame action effects: Theoretical, numerical and practical approaches, *Engineering Structures*, Volume 132, (1 February 2017), Pages 761-777.
- [18]. Yan-Lin.Guo, P.Zhou, M-Z.Wang, Y-L.Pi, M.A.Bradford, J-Z.Tong, Experimental and numerical studies of hysteretic response of triple-truss-confined buckling-restrained braces, *Engineering Structures*, Volume 148,(1 October 2017), Pages 157-174,
- [19]. G. Della Corte, M. D’Aniello, R. Landolfo, Field testing of all-steel buckling restrained braces applied to a damaged reinforced concrete building., (2015) *Journal of Structural Engineering*. Vol. 141, No. 1.
- [20]. J-W. Hu, E. Choi, Seismic design, nonlinear analysis, and performance evaluation of recentering Buckling-restrained Braced Frames (BRBFs), *International Journal of Steel Structures*, Vol 14 (2014), No 4, 683-695.
- [21]. Di Sarno, R. Child, G. Manfred, Seismic response analysis of existing non-ductile buildings retrofitted with BRBS, In: 4th Ecomas Thematic Conference on Computational Methods in Structural Dynamics and Earthquake Engineering, (June 12–14, 2013) Kos Island, Greece.
- [22]. Chung-CheChou, Jia-Hau Liu, Dinh-Hai Pham, Steel buckling-restrained braced frames with single and dual corner gusset connections: seismic tests and analyses, *Earthquake Engineering and Structural Dynamics*, Volume 41 issue 7 , (June 2012) Pages 1137-1156.
- [23]. American Institute of Steel Construction (AISC). Seismic Provisions for Structural Steel Buildings, July 12, 2016, dated June 22, 2010, and all previous versions AISC.341-16.

- [24]. American Institute of Steel Construction (AISC). Seismic Provisions of Structural Steel Buildings, June 22, 2010 dated March 9, 2005.
- [25]. National Earthquake Hazards Reduction Program (NEHRP). Seismic Design of Steel Buckling-Restrained Braced Frames, A Guide for Practicing Engineers, September 2015, NistGcr15-917-34.
- [26]. Z.Q. Jiang, C. Dou, Y.L. Guo, A.L. Zhang, End detailing experimental study of the pinned double-rectangular tube, *Journal of Constructional Steel Research*, Volume 133, (June 2017) Pages 333-344.
- [27]. Z.Q. Jiang, C. Dou, Y.L. Guo, A.L. Zhang, Theoretical study on design methods for pinned assembled BRB with flat core, *Engineering Structures*, Volume 133, (15 February 2017), Pages 1-13.
- [28]. S. b. Momenzadeh, O.Seker, M.Faytarouni, J.Shen, Seismic performance of all-steel buckling-controlled braces with various cross-sections, *Journal of Constructional Steel Research*, Volume 139, (December 2017) Pages 44-61.
- [29]. A.F.Ghowsi, D.R. Sahoo, Experimental study of all-steel buckling-restrained braces under cyclic loading, *International conference on earthquake engineering and structural dynamic*, (12-17 June2017) Reykjavik, Iceland.
- [30]. Sh. Hosseinzadeh, B. Mohebi, Seismic evaluation of all-steel buckling restrained braces using finite element analysis, *Journal of Constructional Steel Research*, Volume 119, (March 2016) Pages 76-84.
- [31]. J. P. Judd, I. Marinovic, M. R. Eatherton, C. Hyder, A. R. Phillips, A.T. Tola, F. A. Charney, Cyclic tests of all-steel web-restrained buckling-restrained brace subassemblages, *Journal of Constructional Steel Research*, Volume 125, (October 2016) Pages 164-172.
- [32]. M.B. Bozkurt, C. Topkaya, Development of welded overlap core steel encased buckling-restrained braces, *Journal of Constructional Steel Research*, Volume 127, (December 2016), Pages 151-164.
- [33]. G. Metelli, G. Bregoli, F. Genna, Experimental study on the lateral thrust generated by core buckling in bolted-BRBs, *Journal of Constructional Steel Research*, Volume 122, (July 2016), Pages 409-420.
- [34]. W. Li, B. Wu, Y. Ding, Experimental performance of buckling-restrained braces with steel cores of H-section and half-wavelength evaluation of higher-order local buckling, *Advances in Structural Engineering*, Volume 20, Issue 4, (2017), page(s): 641-657.
- [35]. N. Hoveidae, B. Rafezy, Local buckling behavior of core plate in all-steel buckling restrained braces, *International Journal of Steel Structures* 15(2): 249-260 (2015), DOI 10.1007/s13296-015-6001-x
- [36]. J. Zhao, B. Wu, W. Li, J. Ou, Local buckling behavior of steel angle core members in buckling-restrained braces: Cyclic tests, theoretical analysis, and design recommendations, *Engineering Structures*, Volume 66 ((1 May 2014) 129-145